Detection of Rapidly Developing Cumulus Areas through MTSAT Rapid Scan Operation Observations

OKABE Izumi*, IMAI Takahito* and IZUMIKAWA Yasushi*

Abstract

The Meteorological Satellite Center (MSC) of the Japan Meteorological Agency (JMA) is currently developing a new product for the detection of rapidly developing cumulus areas (RDCAs) in which cumulus clouds are potentially expected to evolve into thunderstorms within one hour. The method used for this product requires Rapid Scan Operation (RSO) observations by the JMA satellite MTSAT-1R at five-minute intervals. The product detects RDCAs by means of four processes: Detection 1; Motion Cancellation; Detection 2; and Consistency. The Detection 1 process detects developing cumulus areas that are candidates for RDCAs. The algorithm developed for the RDCA product is based on that of the Cloud Grid Information product operationally generated at the MSC. In the Motion Cancellation process, the time trend parameters required for the Detection 2 process are derived. In order to accurately identify time trends in terms of the growth of target clouds, the relative motions of the clouds have to be cancelled. Using these time trend parameters, the Detection 2 process detects vigorously developing cumulus areas from the candidate areas identified in the Detection 1 process. The detection algorithm employs the time trend parameters for the brightness temperature (TB) of infrared (IR) 10.8 μm and those for the visible (VIS) albedo. The time trend parameters for the TB of IR 10.8 μm are based on the detection parameters used for the Convective Initiation product of the European Organization for the Exploitation of Meteorological Satellites (EUMETSAT). Those for the VIS albedo are unique to the RDCA product. The Consistency process ensures that cumulonimbus clouds remain detected while they are in the mature stages of their lifecycle. This process also helps to ensure that the detection results are consecutive, starting from the formation of clouds to the occurrence of severe phenomena. Sample results from the test RSO observations obtained from MTSAT-2 show that the RDCA product has a certain degree of suitability. However, some difficulties regarding the use of this product were also found. This paper also includes a description of the current state of research into the effectiveness of the Motion Cancellation process; an explanation of the slope index; and a discussion of the spatial lag between images from different channels.

1. Introduction

For the first time of the Rapid Scan Operation (RSO) observations at the Meteorological Satellite Center (MSC) of the Japan Meteorological Agency (JMA), the extra observations of typhoons were carried out by Geostationary Meteorological Satellite 3 (GMS-3). These observations were conducted at 15-minute intervals. MTSAT-2 was used to conduct special observations at 4- and 7-minute intervals for The Observing-system Research and Predictability Experiment (THORPEX). The Atmospheric Motion Vectors (AMVs) derived from the RSO observations have been found to contribute to the more accurate forecasting of typhoon tracks

*System Engineering Division, Data Processing Department, Meteorological Satellite Center

（Received June 24, 2010, Accepted December 15, 2010）

(Nakamura et al. 2002).

On 1 July 2010, the JMA switched satellite operations over from MTSAT-1R to MTSAT-2. After that, MTSAT-1R entered standby mode. Using this satellite, Test RSO observations were conducted in the summer and autumn of 2010, and plans are underway for routine RSO observations to be conducted mainly during the daytime every summer from 2011.

RSO observations provide information at frequent intervals on rapidly changing phenomena such as cumulonimbus (Cb) development. Using these data, the MSC have been developing a new product for the detection of rapidly developing cumulus areas (RDCAs) in which cumulus clouds are potentially expected to evolve into thunderstorms within one hour. The Convective Initiation (CI) product provided by the European Organisation for the Exploitation of Meteorological Satellites (EUMETSAT) was referred to in the development of this product. The CI product identifies rapidly growing cumulus that may potentially evolve into strong convective storms within one hour. Since the RDCA product will also be provided to aviation users, thunderstorms that can have a disastrous effect on aviation safety are targeted for detection by means of this product. This information will be provided to aviation users in the future via the MetAir system, which is a web-based service developed by the JMA for the provision of information on aviation safety. The algorithm, the definition of the detection parameters, and the method of verifying the validity of the algorithm are currently under development.

Verifications have been conducted to date only for case studies drawn from areas over land. However, the MSC will refine the product so that it can also be applied for ocean areas, since radar networks, which are already used to provide information about severe convections over land, have not covered ocean areas.

This paper outlines the current progress that has been made in the development of the RDCA algorithm, and examines some of the results that have been obtained. Section 2 details the data used for the RDCA product and those used to verify the results of this paper. Section 3 presents an outline of the algorithm. Section 4 describes the method used to derive the slope index. Section 5 presents and discusses examples of the RDCA product. Section 6 describes a study on the effectiveness of the Motion Cancellation process and the slope index. Finally, section 7 provides a summary of this paper.

2. Data

2.1 MTSAT-1R RSO data

RSO data from MTSAT-1R provides observation images taken at frequent intervals of five minutes over a limited area that includes almost all of Japan.

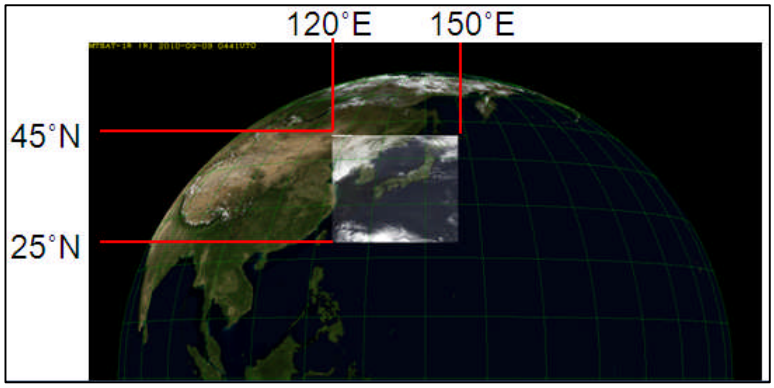

Fig. 1 An example of an RSO observation image taken by MTSAT-1R

Table 1　The wavelengths and spatial resolutions of the MTSAT-1R/2 image

Channel	VIS	IR 10.8 μm	IR 12.0 μm	WV 6.8 μm	Near-IR 3.8 μm
Wavelength (μm)	0.55-0.90	10.3-11.3	11.5-12.5	6.5-7.0	3.5-4.0
Resolution at SSP (km)	1	4	4	4	4

The observation area is scheduled to cover the region from 25 to 45°N and from 120 to 150°E, as shown in Fig. 1. The RSO data channels are the same as those used for the global observations conducted until 1 July 2010. Table 1 shows the wavelengths for these channels. The spatial resolutions of the RSO images are also the same as those used for the global observations; namely, 1 km for the visible (VIS) channel and 4 km for the infrared (IR) channels at the sub-satellite point (SSP). The RDCA product requires data from all five channels.

2.2　LIDEN data

In this paper, data from the Lightning Detection Network (LIDEN), radar echo data, and data from the JMA's archives of information on tornadoes and other hazardous winds are used to verify the accuracy of the calculation results. LIDEN is a JMA network system that is used to observe the time, position, and type of thunder-related phenomena by detecting radio waves caused by lightning flashes. Types of thunder-related phenomena include the following: cloud-to-ground strokes and cloud-to-cloud lightning. Only observations of strokes are used for verification in this product since observations of cloud-to-cloud lightning are not very accurate in terms of its location.

2.3　Radar systems

There are twenty radar systems that cover almost all of Japan. Composed data on the estimated surface precipitation (as precipitation intensity) and three-dimensional radar echo data (as radar echoes) are available. These two types of data are available every 10 minutes (every 5 minutes since July 2009) through the Radar Information Sharing System (RISS). Horizontal cross-sections of the radar echoes are available at altitudes ranging from 1 to 15 km at an interval of 1 km, and vertical cross-sections are available for all corresponding lines on the horizontal maps.

2.4　Tornado observations

The JMA's archives of information on tornadoes and other hazardous winds are repositories for manually collected research data obtained by the JMA. The archives contain a record of where a tornado struck, the time and date at which it struck, and its scale.

2.5　Data from NWP

Certain instability indexes are used to discuss meteorological conditions. Grid Point Values (GPVs) from Numerical Weather Prediction (NWP) data are used to calculate CAPE (convective available potential energy). SSI (Showalter Stability Index) and SSI*[1] are calculated from radiosonde observations.

[1] An instability index that is equal to the SSI when the air at the bottom layer is saturated.

3. Algorithm

As shown in Fig. 2, the RDCA product consists of the following four processes: Detection 1; Motion Cancellation; Detection 2; and Consistency. As preparation for the main processes, the data obtained from the five channels are inserted for 0.01 × 0.01° grid data sets from 20 to 50°N and from 120 to 150°E for each observation time using the nearest neighbor method. Fig. 3 shows the life cycle of a Cb. The four clouds in the left-hand side of Fig. 3 represent cumulus clouds in the cumulus stage. These are selected through the Detection 1, Motion Cancellation, and Detection 2 processes. Cumulonimbus clouds in the mature stage, as represented by the fifth cloud from the left in Fig. 3, are detected through the Consistency process using the latest RDCA results. The Consistency process also helps to stabilize the detection results through all of the thunderstorm lifecycle.

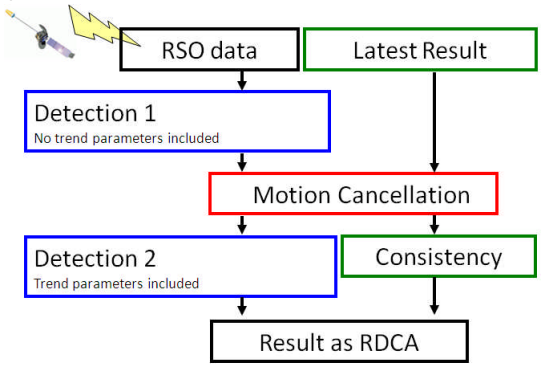

Fig. 2 Flow of the RDCA product

3.1 Detection 1

The Detection 1 process is designed to identify cumulus cloud areas in the cumulus stage as the candidates for RDCAs. As shown in Table 2, four check items and eight parameters are used for this process. Parameters 1 and 6 are used for the computation of the Cloud Grid Information (CGI) product (Tokuno 2002; Mouri and Terasaka 2008) used at the MSC to detect convective cloud areas. Parameters 2, 3, 4, and 7 were introduced based on the parameters used to distinguish cumulous clouds from stratocumulus clouds in the CGI product. The other parameters are unique to the RDCA product.

Each condition is checked for every grid in the 3000 × 3000 grid data set, which corresponds to the area from 20 to 50°N and from 120 to 150°E. The MAX and MIN variables in the table are the maximum and minimum values, respectively, that are obtained from grids within a 7 × 7 grid area, and the AVERAGE variable and the standard deviation are calculated using values obtained from within a 21 × 21 grid area surrounding the grid in question. The size of the 7 × 7 grid area is the same as that of the template used in the Motion Cancellation process, while the size of the 21 × 21 grid area is determined based on the target phenomena's scale.

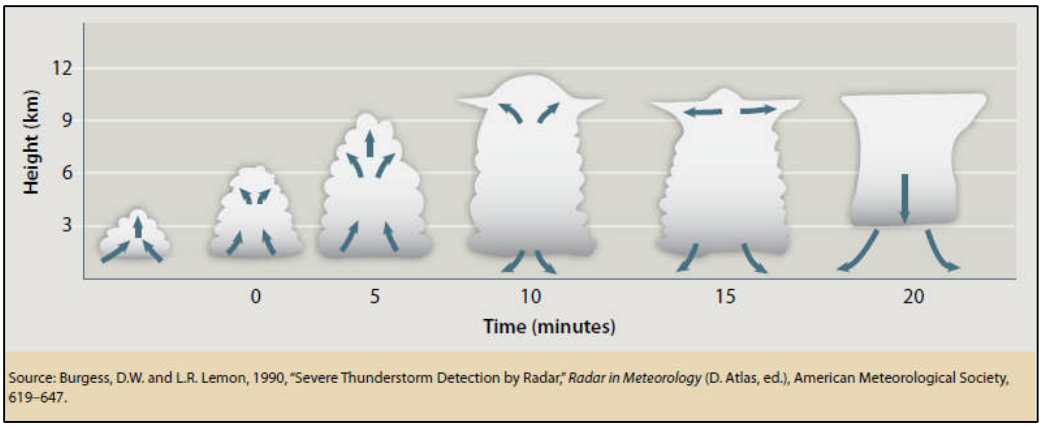

Fig. 3 A concept model of the thunderstorm lifecycle (E. Brotack, 2009, "Nasty Surprise", AeroSafety World, October 2009, Flight Safety Foundation)

Table 2　Parameters and conditions for the Detection 1 process

	Parameters	Conditions	Check items
P1	Vis. Albedo / cos(sunZenithAngle)	1-1 (TH_min < P1 only)	Check 1: Optical thickness
P2	Vis. Albedo_MAX - Vis. Albedo_AVERAGE	1-2 (TH_min < P2 only)	Check 2: Cloud texture
P3	Standard deviation of Vis. Albedo	1-3 (TH_min < P3< only)	Check 2: Cloud texture
P4	TB 10.8_MIN - TB_10.8_AVERAGE	1-4 (TH_min < P4 < TH_max only)	Check 2: Cloud texture
P5	Standard deviation of TB 10.8	1-5 (TH_min < P5< only)	Check 2: Cloud texture
P6	TB difference IR 10.8 - IR 12.0	1-6 (P6 < TH_max only)	Check 1: Optical thickness
P7	TB difference WV 6.8 - IR 10.8	1-7 (TH_min < P7 < TH_max only)	Check 3: Depth between cloud tops and the tropopause
P8	Slope Index	1-8 (TH_min< P8 only)	Check 4: Updraft in clouds

(The MAX and MIN variables are calculated using grids within a 7 × 7 grid area. The AVERAGE variable and the standard deviation are calculated from values within a 21 × 21 grid area.)

Check 1 is conducted to select cumulus cloud from all of the grid data, taking advantage of the fact that cumulus clouds have a higher optical thickness than low stratus clouds and thin cirrus clouds (MSC 2002). Parameter 6 has a large value over optically thin cloud areas since water and ice clouds have a higher absorption in the IR 12.0 μm channel than in the IR 10.8 μm one and it provides a useful means of eliminating optically thin clouds. In Check 2, the texture of the cloud top surface is checked to determine whether it is as rough as that of cumulus clouds. In Check 3, a test is conducted to determine whether the clouds have the potential to further grow in height. Water Vapor (WV) 6.8 μm channel is more sensitive to water vapor than IR 10.8 μm, and there is a larger amount of water vapor in the troposphere than in the stratosphere. The brightness temperature (TB) of WV 6.8 μm is much lower than the TB of IR 10.8 μm when the depth between the tropopause and cloud tops is large. Parameter 7 can serve as an indicator of this depth, which is considered to represent the potential for height growth. The updraft strength in relation to the convection intensity in clouds is checked using the slope index described in section 4. The condition thresholds given in Table 2 (i.e. the TH_min and TH_max variables) are, at present, decided subjectively based on an analysis of sample cases from 2008 and 2009. During this period, RSO data are obtained from MTSAT-2. The MSC will re-evaluate these thresholds statistically using RSO data obtained from MTSAT-1R in 2010.

3.2　Motion Cancellation

The Motion Cancellation process is conducted to calculate the time trend parameters required for the Detection 2 process. In order to accurately identify time trends in terms of the growth of target clouds, the relative motions of the clouds have to be cancelled. In the RDCA product, the cross-correlation coefficient method is used for the Motion Cancellation process. This technique is generally adopted for the AMV products not only at the MSC/JMA, but also at most other satellite centers (Oyama R. 2010). It is used to identify a certain size of segment (called a template) in a base image, using the segment with the pattern that most closely corresponds to the image targeted for comparison. The similarity is calculated using correlation coefficient values.

A unique feature of the RDCA product is its use of three successive VIS images for the cross-correlation coefficient method (Shimoji K. 2010), while only two successive images are generally used for the AMV product (Fig. 4). Three successive images—A (the first image), B (the second image, which serves as the base image) and C (the third image)—are used to obtain two series of correlation coefficient values: $CC_{BA}(pix_B, lin_B, \Delta pix_{BA}, \Delta lin_{BA})$ and $CC_{BC}(pix_B, lin_B, \Delta pix_{BC}, \Delta lin_{BC})$. In Fig. 4, (pixA, linA), (pixB, linB), and (pixC, linC) represent the template's center grid in Image A, Image B, and Image C, respectively. These images are selected so that (pix_A, lin_A), (pix_B, lin_B), and (pix_C, lin_C) have geographically the same coordinate origins. These values are combined to create a new series of values named CC_O, as shown in equation (3.2.1) below.

$$CC_O = CC_{BC}\left(pix_B, lin_B, \Delta pix_{BC}, \Delta lin_{BC}\right) + CC_{BA}\left(pix_B, lin_B, \Delta pix_{BA}, \Delta lin_{BA}\right) \quad (3.2.1)$$

Here, target clouds are assumed to move uniformly during the observations of the three images. The center grids (pixB, linB) and (pixC, linC) are identified according to where the CC_O value is highest, and the time trend is calculated using the relevant values for the two grids.

VIS albedo images are used in this process, since the spatial resolution of VIS observations is higher than that of IR observations. The higher the image resolution is, the more precise tracking result will be obtained. In addition, the product targets convective clouds, so VIS images are the most suitable data for the Motion Cancellation process.

A template size of 7 × 7 pixels and a search area size of 19 × 19 pixels were provisionally adopted. A smaller template size would prevent contamination by the different motions of the surrounding clouds, while a larger one would contain sufficient information to estimate the image pattern similarity, and the reliability of the tracking would be enhanced. Given this, the developer adopted a trial and error approach to determining the template size. A search area size of 19 × 19 pixels was decided on based on the assumption that the target clouds will move no faster than 30 m/s. Within a search area of this size, a template of 7 × 7 pixels can move a maximum of 6 pixels eastward or westward and 6 pixels northward or southward. Since 1 pixel (0.01 degrees longitude/latitude at the SSP) corresponds to between about 1 and 1.5 km at the mid-latitude location, 6 pixels correspond to between about 6 and 9 km. Given that RSO observations are conducted at 5-minute intervals, the motion speed of a target that moves 9 km from one image to the next is estimated to be about 30 m/s.

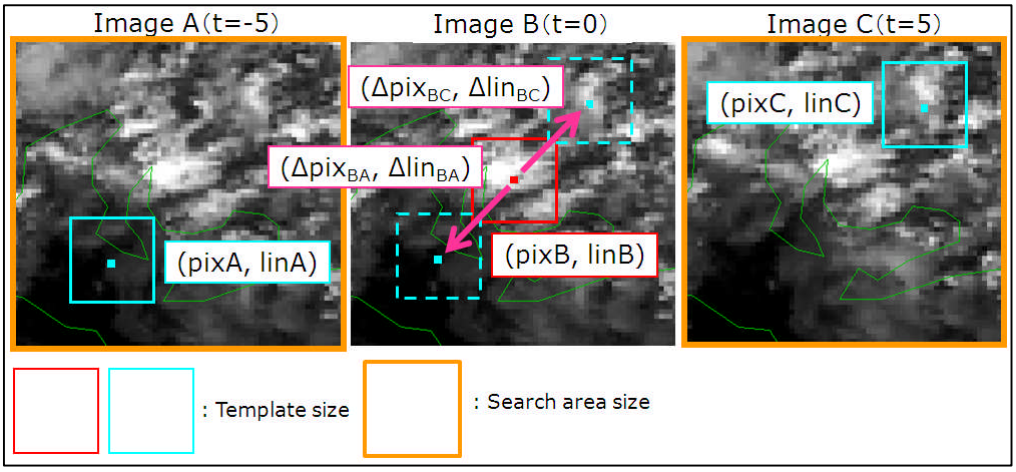

Fig. 4 Three successive images as used in the cross-correlation coefficient method

Table 3　Parameters and conditions for the Detection 2 process

	Parameters	Conditions	Check terms
P9	Time trend of Vis. Albedo_MAX	2-1 (TH_min < P9 OR TH_min < P10)	Check 5: The time trend of optical thicknesses
P10	Time trend of Vis. Albedo_AVERAGE		
P11	Time trend of TB 10.8_MIN	2-2 {(TH_min < P11 < TH_max AND TH_min < P13 < TH_max) OR TH_min < P12 < TH_max }	Check 6: The time trend of cloud height
P12	Time trend of TB 10.8_AVERAGE		
P13	Pinpoint fall down of TB 10.8		

3.3　Detection 2

In the Detection 2 process, vigorously developing cumulus areas are detected from the candidate areas selected during the Detection 1 process. As shown in Table 3, two check items and five parameters are used for the process. Parameters 11 and 12 were introduced based on the parameters used for EUMETSAT's CI product. The other parameters are unique to the RDCA product.

In Check 5, vigorously developing cumulus clouds are detected by means of the albedo of the cloud top surface. When a convective cloud is rapidly developing, the albedo of its top surface rapidly increases. In order to detect the same targets Check 6 requires the time trend for the TB of IR 10.8 μm. Areas in which cloud tops are rapidly growing in height are the regions in which the TB of IR 10.8 μm is quickly decreasing.

In order to estimate the growth of a target cell's height accurately, it is necessary not only to conduct the Motion Cancellation process, but also to give consideration to cell transformations on a smaller scale than that allowed for by the template size. The time trend for the maximum VIS albedo (i.e. parameter 9) and the time trend for the minimum TB of IR 10.8 μm (i.e. parameter 11) can indicate the time trend for a cell's height, even if the cell transforms in such a small scale that it is not allowed for by the template size.

3.4　Consistency

The Consistency process is the last of the four processes conducted for this product. As shown in Fig. 3, the height of a cumulus cloud increases greatly while it is in the cumulus stage of its lifecycle. Target cumulus clouds in this stage are detected through the Detection 1, Motion Cancellation, and Detection 2 processes. However, thunderstorms continue to affect aviation safety in the mature stage (i.e. when the clouds are fully developed). The Consistency process ensures that critical Cbs remain marked while they are in the mature stage. When previously identified cloud grids are no longer detected, this process works to check whether those clouds are actually dissipating. In addition, since clouds do not develop in nature at a fixed rate, some cloud areas will be detected intermittently through the Detection 1, Motion Cancellation, and Detection 2 processes. The Consistency process also helps to stabilize the detection results during the period from the formation of a cloud area through to the occurrence of severe phenomena.

Table 4 shows the parameters and conditions used for this process. Due to the purpose of this process, the following parameters are not used for the Consistency process: parameters 3 to 5 (which are related to checking the roughness of cloud texture) and parameters 9 and 10 (which are related to checking for increases in the

Table 4 Parameters and conditions for the Consistency process

	Parameters	Conditions	Check items
P9	Time trend for Vis Albedo_MAX	2-1 (TH_min < P9 OR TH_min < P10)	Check 5: Time trend of optical thicknesses
P10	Time trend for Vis Albedo_AVERAGE		
P11	Time trend for TB 10.8_MIN	2-2 {(TH_min < P11 < TH_max AND TH_min < P13 < TH_max) OR TH_min < P12 < TH_max }	Check 6: Time trend of cloud height
P12	Time trend for TB 10.8_AVERAGE		
P13	Pinpoint fall down for TB 10.8		

optical thickness of clouds). Investigations using RSO data in 2008 to 2009 revealed that these parameters had no effect on the detection of thunderstorms after a cloud develops an anvil head. A fully developed cumulus in the mature stage (i.e. Cb) already has a high optical thickness, and the time trend for the VIS albedo is very small. Grids which meet the conditions stipulated for the Consistency process are considered to contain RDCAs.

After the four processes have been conducted, VIS albedos for the 21 × 21 grid area surrounding grids that have been identified as RDCAs are checked. Surrounding grids with albedo values higher than 0.54 × cos(sunZenithAngle) are also considered as a part of RDCAs.

4. Slope index

The slope index (parameter 8 in Table 2) is used as an indicator of updraft strength. This index was originally introduced in the RDCA product based on the Rosenfeld Lensky Technique (RLT), which is used to gain insights into precipitation formation processes through satellite observations (Rosenfeld and Lensky 1998). As shown in Fig. 5, particles in cloud tops with strong updrafts are smaller than those in cloud tops with weak updrafts at the same altitude. This theory assumes that the bottoms of these clouds are at the same altitude (Lindsey et al. 2006). Particles in strong updrafts are raised upward in such a short time that they can reach the top before they

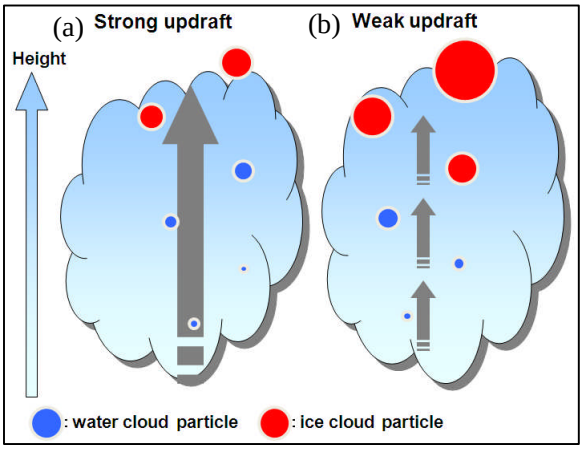

Fig. 5 Particles in clouds with strong and weak updrafts

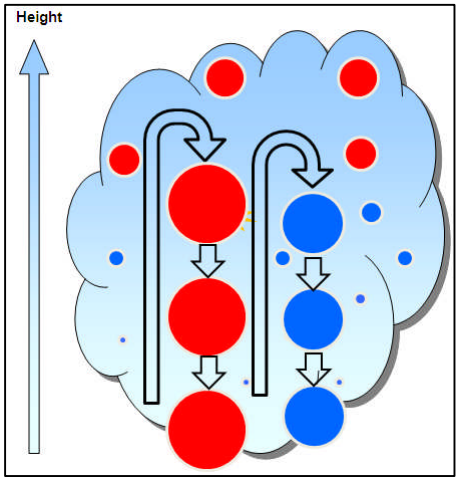

Fig. 6 Same as Fig. 5 but with hail and large precipitation particles also shown

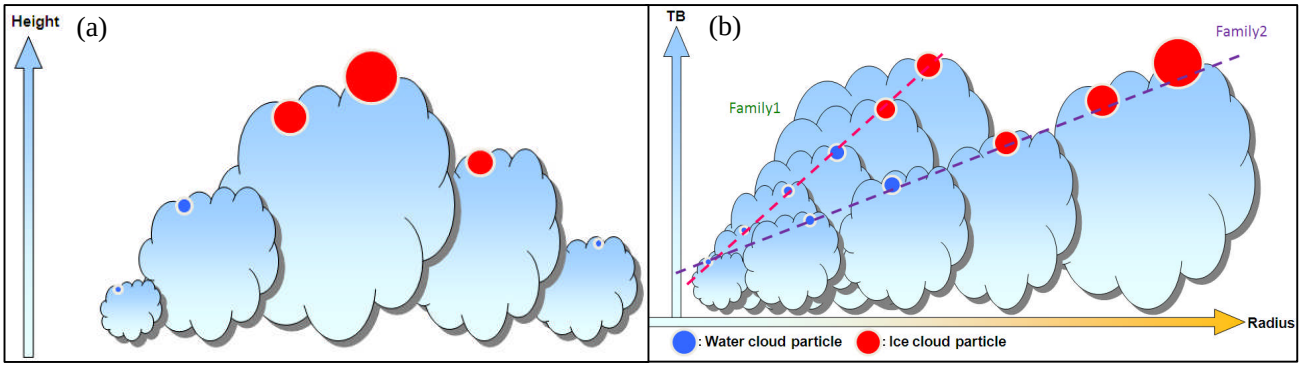

Fig. 7　Same as Fig. 5 but with only particles in the cloud tops shown. The figure on the right is a diagram showing cloud-top particles in two families, with the vertical axis representing the TB IR 10.8 μm and the horizontal axis representing the particle radius.

grow in their radius very much (Fig. 5). Hailstones or large rain particles that are present in a cloud fall before they reach its top, so they cannot be observed by a satellite (Fig. 6). It should be noted that the situation illustrated in Fig. 5 does not hold true for all cloud particles; it depicts only those that reach the cloud top. Adjoining clouds are considered to be part of the same cloud family and to grow according to the same lifecycle (Fig. 7(a)). Each family contains clouds of varying heights. Fig. 7(b) shows how the TB of IR 10.8 μm varies according to the radius of particles in a strong updraft family (Family 1) and that of particles in a weak updraft family (Family 2). The slope for Family 1 is steeper than that for Family 2. Since the TB of IR 10.8 μm corresponds to cloud height and the particle radius corresponds to time, the slope corresponds to the updraft speed. This ergodic theory (the essence of the exchangeability of time and space for the TB-radius relationship in convective clouds) is outlined by Lensky and Rosenfeld (2006).

As it is not practical to observe the individual radii of cloud particles directly using MTSAT satellites, the effective radii are adopted for this method. In order to estimate the effective radii, equations (4.1.1) and (4.1.2) are used (Oku and Ishikawa 2008).

$$\ln(A_{38}) = a_0 + a_1 \times R_e + a_2 \times R_e^{\,2} + a_3 \times R_e^{\,3} \quad (4.1.1)$$

$$\begin{cases} a_0 = -0.68460 \\ a_1 = -0.08243 \\ a_2 = -0.00749 \\ a_3 = 0.00033 \end{cases} \quad (4.1.2)$$

where A_{38} is the albedo at 3.8 μm and R_e is the effective radius. a_0, a_1, a_2 and a_3 are constant parameters. Oku and Ishikawa noted that (4.1.1) and (4.1.2) are suitable only for water particles in optically thick clouds. Clouds that satisfy conditions 1-1 to 1-7 (Table 2) are considered to form optically thick clouds. Parameter 8 is not calculated when a grid has a TB of IR 10.8 μm of less than 250 K, because clouds of such a low temperature will consist of ice particles rather than water particles.

Similar to the approach used by Lindsey et al. (2006), the following method is used to derive A_{38}. During the day, radiance observed at 3.8 μm includes both that emitted from the Earth's atmosphere and reflected solar radiation. This can be described as outlined in equation (4.1.3) below.

$$R_{38} = A_{38} \times R_{38i} + (1 - A_{38}) \times R_{38e}(T) \quad (4.1.3)$$

where R_{38} is the total radiance at 3.8 μm, R_{38i} is the solar flux at the top of the atmosphere, and $R_{38e}(T)$ is the blackbody radiance at 3.8 μm at temperature T. In this

method, the emission temperature at 10.8 μm is used for $R_{38e}(T)$, since this value is approximately equal to that at 3.8 μm for optically thick clouds. Here, the transmittance at 3.8 μm is considered to be zero for optically thick clouds. Equation (4.1.4) below can be obtained from equation (4.1.3).

$$A_{38} = (R_{38} - R_{38e}(T))/(R_{38i} - R_{38e}(T)) \qquad (4.1.4)$$

Here, R_{38i} is given by equation (4.1.5) below.

$$R_{38i} = r_{sun}^{\ 2} \times R_{38s} \times COS\,(sunZenith\,)/d^{\,2} \qquad (4.1.5)$$

where r_{sun} is the radius of the Sun, R_{38s} is the blackbody radiance of the Sun, and d is the radius of the Earth's orbit.·

The slope index is composed of the R_e and the TB of IR 10.8 μm within a 21 × 21 grid segment surrounding the grid in question, and is defined as shown in equation (4.1.6) below. In order to calculate the inclination, the reduced major axis approach is used (Sokal and Rohlf 1995).

Slope Index

$$\equiv \arctan\left(\frac{\sqrt{\sum_{i=1}^{21}\sum_{j=1}^{21}(TB_{10.8\{i,j\}} - \overline{TB_{10.8}})^2}}{\sqrt{\sum_{i=1}^{21}\sum_{j=1}^{21}(R_{e\{i,j\}} - \overline{R_e})^2}}\right) \qquad (4.1.6)$$

where $TB_{10.8\{i,j\}}$ is the TB of IR 10.8 μm.

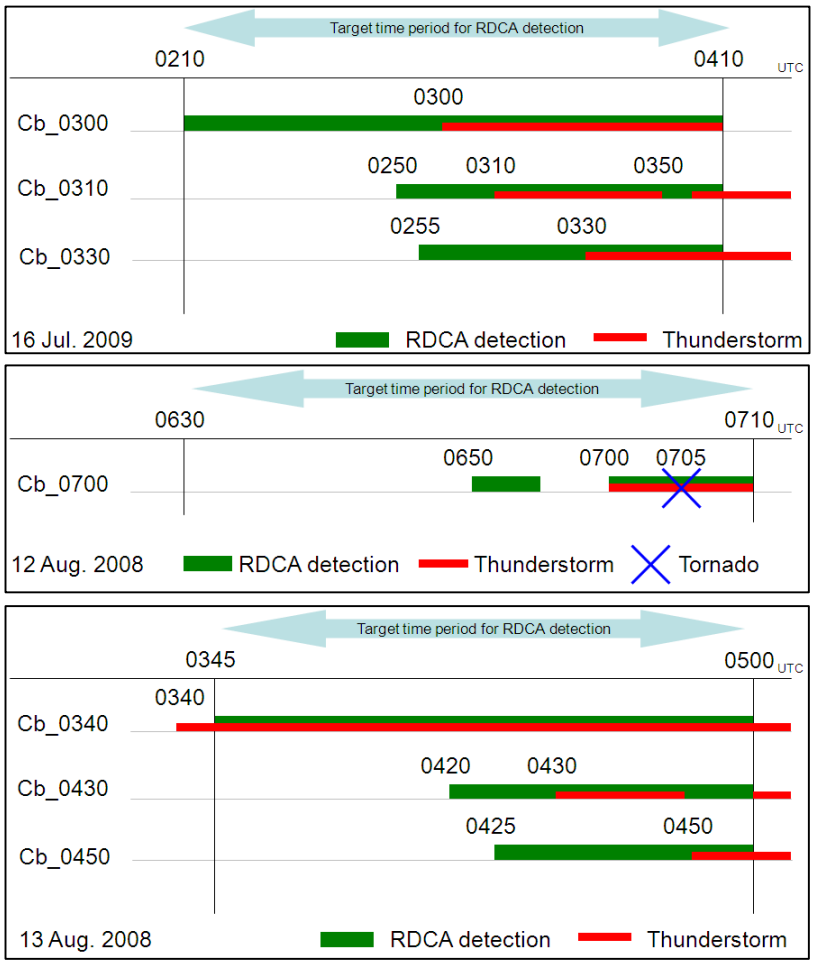

Fig. 8 Thunderstorm durations and RDCA product results for each target on 16 July 2009 (upper), 12 August 2008 (middle) and 13 August 2008 (bottom)

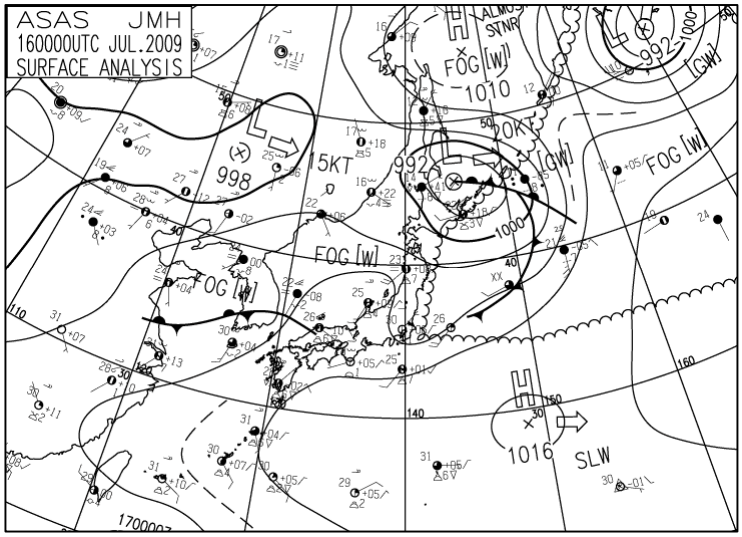

Fig. 9　Weather Chart for 0000 UTC on 16 July 2009

5. Results

In this section, four days' worth of examples are presented for comparison with radar echoes, precipitation intensity, LIDEN data, and the JMA's archives of information on tornadoes and other hazardous winds. Only stroke data informed by the LIDEN data were used to confirm that convective clouds developed into thunderstorms. Each target cloud area is named according to the time at which the thunderstorm began; for example, Cb_0300 would be the name given to a target cloud area that developed into a thunderstorm at 0300 UTC. Fig. 8 shows the duration of thunderstorms and RDCA product results for 12 and 13 August 2008 and 16 July 2009.

5.1　Case study #1: 16 July 2009

The target time was from 0200 to 0410 UTC (11:00 to 13:10 JST[2]) on 16 July 2009. The target area was from 30 to 35˚N and from 127 to 133˚E over the Kyushu area. The weather chart for 0000 UTC on this day is shown in Fig. 9. A stationary front extended from the eastern area of China to the Chugoku area in Japan. Kyushu was located in the rear of high pressure over the Pacific Ocean. According to the analysis chart, warm and wet air was present over the Kyushu area at the 850 hPa level.

CAPE values for over all of Kyushu except for the northeast were larger than 600. Under such unstable conditions, three thunderstorms formed in the Kyushu area during the target time period: Cb_0300, Cb_0310, and Cb_0330. The figures on the right in Fig. 10 show precipitation intensity distributions and LIDEN data. A heavy precipitation area that corresponded to the stationary front was present in the north of Kyushu. Many strokes were observed over this area. The figures on the left in Fig. 10 show the results described on VIS images. RSO observations began at 0200 UTC. Since three images are necessary for the Motion Cancellation process, results were available from 0210 UTC. Three Cbs that developed over Kyushu were successfully detected by the RDCA product. Except for at the edge of the front, however, no Cbs were detected on the stationary front. Since most clouds on the front had merged with surrounding clouds and were concealed by cirrus clouds, it was hard to detect Cbs there by satellite data. This means that the detection algorithm used for the RDCA

[2] JST (Japan Standard Time) is 9 hours ahead of UTC.

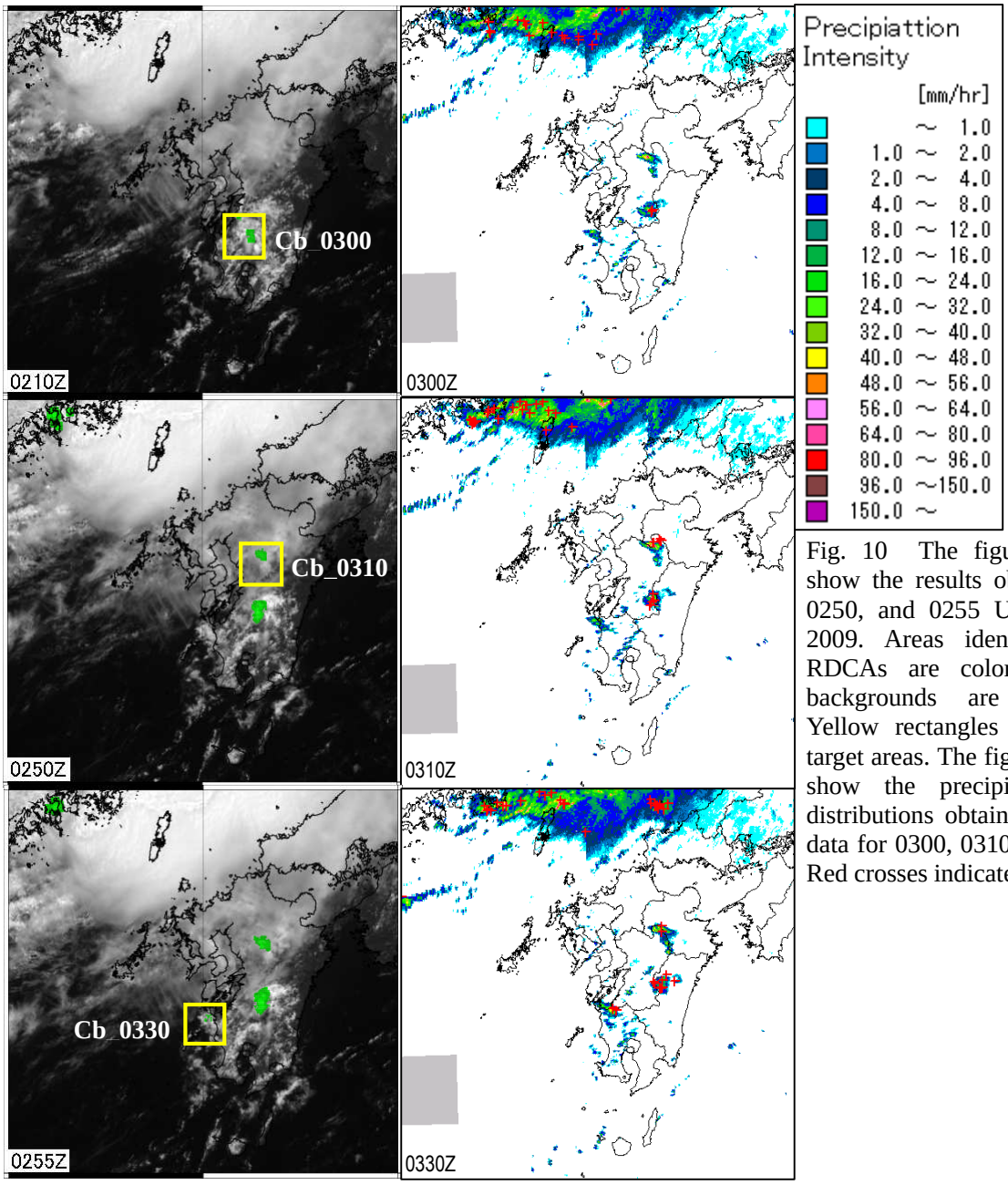

Fig. 10 The figures on the left show the results obtained at 0210, 0250, and 0255 UTC on 16 July 2009. Areas identified as being RDCAs are colored green. The backgrounds are VIS images. Yellow rectangles mark the three target areas. The figures on the right show the precipitation intensity distributions obtained from LIDEN data for 0300, 0310 and 0330 UTC. Red crosses indicate strokes.

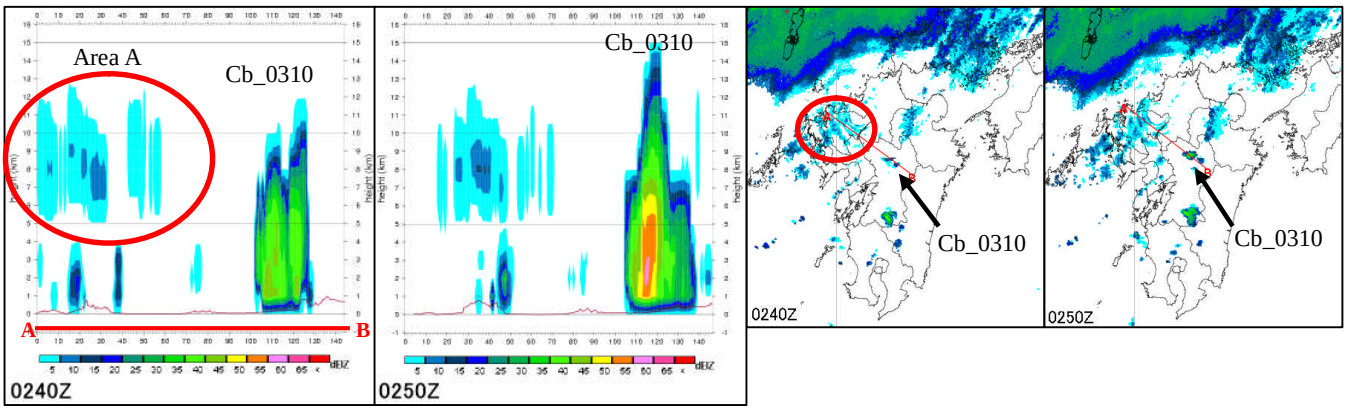

Fig. 11 The figures on the left show vertical cross-sectional views of radar echoes. Their locations are indicated with red lines in the figures on the right. The cirrus cloud areas are marked with red circles.

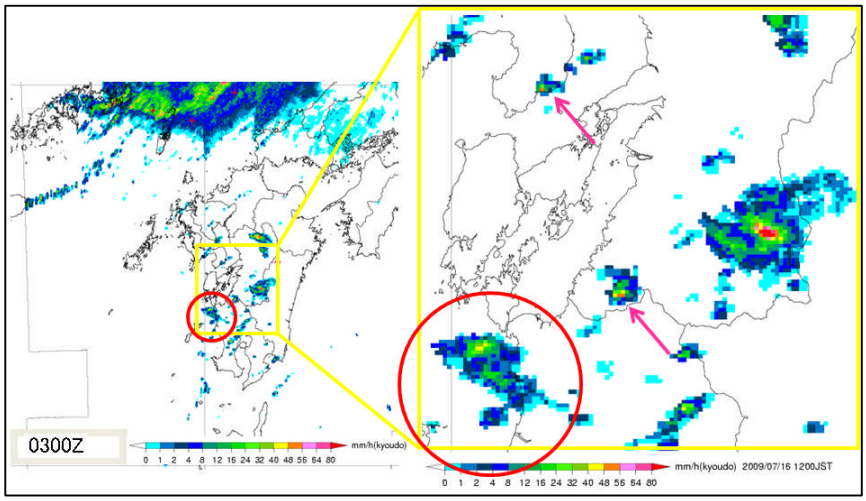

Fig. 12　Precipitation intensity distributions at 0300 UTC (pink arrows indicate extremely intense echoes around Cb_0330.)

product is only able to detect isolated cumulus clouds.

Cb_0300 was detected at 0210 UTC with a lead time of 50 minutes. The maximum precipitation intensity at that time was about 32 to 40 mm/h, but the intensities in most other areas were under 8 mm/h that was too weak to suggest the cell would develop into a Cb. This is a typical successful case for the RDCA product. Cb_0310 was detected with a lead time of 20 minutes, which was shorter than the lead times for the other two cells. Condition 1-5 (the standard deviation for the TB of IR 10.8 μm) and condition 2-2 (the time trend for the TB of IR 10.8 μm) were not met until 0250 UTC, while the other conditions were met from 0240 UTC. The echo-top of Cb_0310 was about 12 km (Fig. 11) at that time. The radar did not detect any cirrus cloud around Cb_0310. However, the TB of IR 10.8 μm over Cb_0310 was the same as that over the upper-echoes observed nearby Cb_0310 (Area A, which is marked with a red circle, in Fig. 11). The time series for the VIS albedo images shows that uniform cirrus clouds moved south-southeast over Area A and Cb_0310. Upper winds of about 300 hPa were south-southeast according to the radiosonde data for Fukuoka at 0000 UTC. According to these situations, certain silky cirrus cloud over Cb_0310 is presumed to have prevented Cb_0310's detection until the top of the Cb was higher than 13 km which is the altitude of the upper-echoes' top. The cirrus cloud was so thin that it did not contaminate the VIS albedo images, which contain information on the target cell, but the TB of IR 10.8 μm is more sensitive to cirrus clouds. Cb_0330 was detected at 0300 UTC with a lead time of 30 minutes. There were some rainy areas around it, and two of them had higher precipitation intensities than Cb_0330 at that time (Fig. 12). This means that the product was able to detect Cb_0330 from among other cells with similar precipitation intensities.

5.2　Other case studies

(a) Case study #2: 12 August 2008

On this day, some tornadoes developed in the northern part of Kyushu at between about 0705 and 0710 UTC (16:05 and 16:10 JST). The weather chart for 0600 UTC is shown in Fig. 13. The tornado (marked with a red circle in Fig.14) first formed to the southeast of a cyclone in the Tsushima Strait that was moving northeast. The CAPE values for over that area suddenly increased from

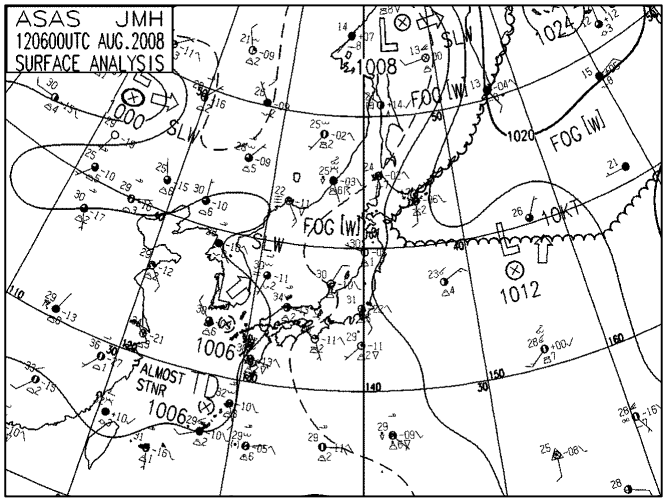

Fig. 13 Weather Chart for 0600 UTC on 12 August 2008

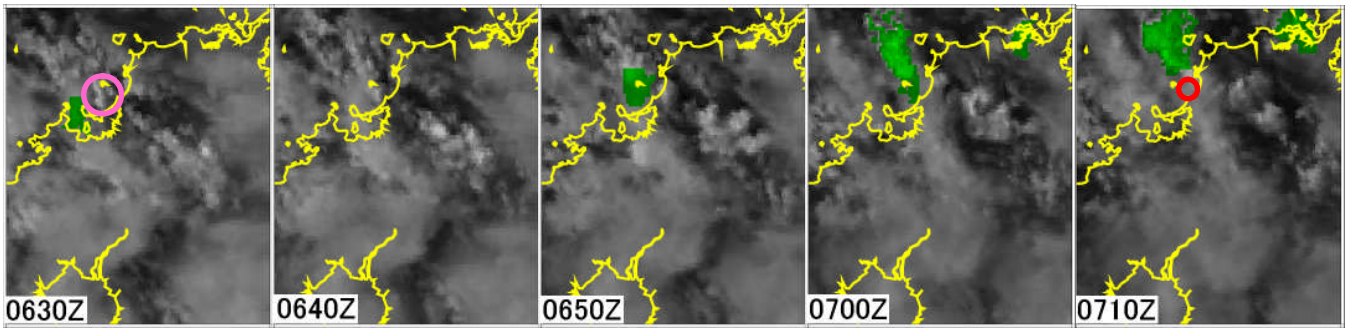

Fig. 14 Same as the figures on the left in Fig. 10 but for the northern part of the Kyushu area between 0630 and 0710 UTC on 12 August 2008. The coastlines have been highlighted in yellow. The red circle indicates where the tornado occurred at 0705 UTC. The pink circle indicates the position of Cb_0700 at 0630 UTC.

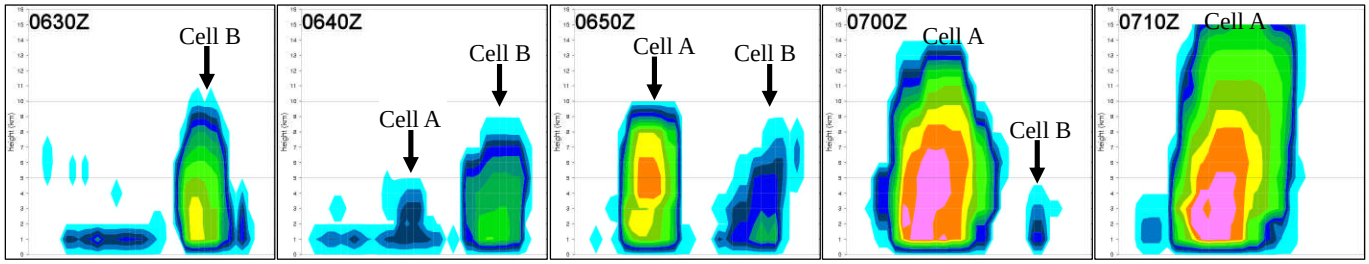

Fig.15 Vertical cross-sectional views of radar echoes. Their locations are indicated with red lines in Fig.15.

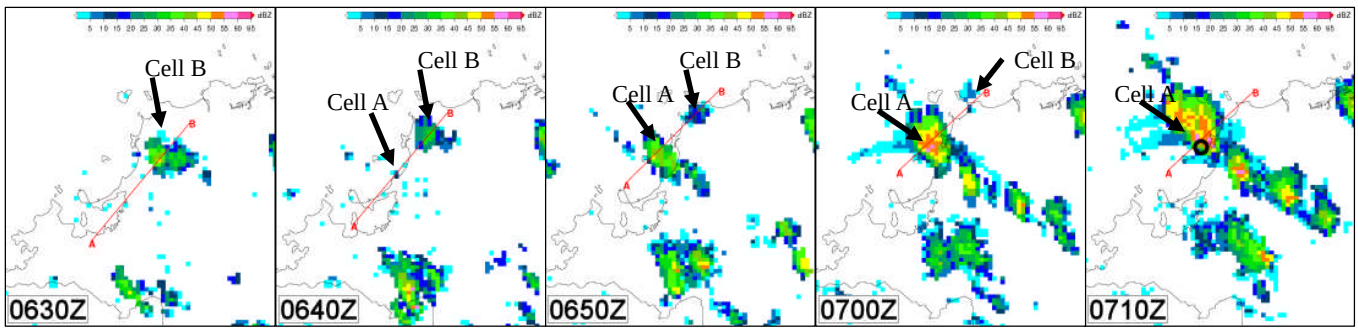

Fig.16 Radar echoes for a 2 km-high plane for the same area and times as for Fig. 15. The black circle denotes the same spot as the red circle at 0710 UTC in Fig. 14.

between 0600 and 0700 UTC. The target area was 33 to 34˚N and 133 to 134˚E over the northern part of Kyushu. The target area corresponding to where the tornado occurred was named Cb_0700. The target time was from 0620 to 0710 UTC, and results were available from 0630 UTC. Cb_0700 was identified as a RDCA at 0650 UTC, which was about 15 to 20 minutes before the tornado occurred (Fig. 14). Cb_0700 had no precipitation until 0650 UTC (not shown); however, vertical cross-sectional views of radar echoes show the development of the cell (Fig. 15). Cb_0700 (labeled Cell A in Figs. 15 and 16) rapidly developed in contrast to the neighboring cell (labeled Cell B in Figs. 15 and 16), which rapidly declined. Fig. 15 shows the explosive development of the cloud height of Cb_0700 between 0640 and 0650 UTC. The cloud area detected at 0630 UTC did not correspond to Cb_0700. The detected cloud moved southeast according to the time series for the VIS images, and the radiosonde data for Fukuoka at 0000 and 1200 UTC suggest its movement was identical to that of upper clouds. The cloud area that corresponds to Cb_0700 is marked with a pink circle in the figure for 0630 UTC in Fig. 14. The surrounding upper clouds prevented its detection from 0630 to 0645 UTC. Because of the presence of these upper clouds, parameter 3 (the standard deviation for the VIS albedo) did not meet the threshold value. It is extremely regrettable when the failure to detect an RDCA is the result of only one condition. This case made us aware that regarding cloud areas as RDCAs only when all the condition thresholds strictly meet could result in some RDCAs being overlooked.

(b) Case study #3: 13 and 14 August 2008

For the 13 August 2008 case study, the target times were from 0220 to 0310 UTC and from 0345 to 0500 UTC (11:20 to 12:10 JST and 12:45 to 14:00 JST, respectively). The results for between 0315 and 0340 UTC are not available due to a lack of observations from 0315 to 0330 UTC. The target area was 35 to 38˚N and 136 to 140˚E over the Kanto area. The weather chart for 0600 UTC is shown on the left in Fig. 17. There was a high pressure zone over the sea to the south of Japan, and the pressure gradient over the Kanto area was gentle. Most of the surface temperatures in the target area were above 30°C at 0400 UTC. The figures in the bottom row in Fig. 18 show the precipitation intensity distributions and LIDEN data. Three cumulonimbus clouds developed during the target time: Cb_0340 in the western part of the Tokyo metropolis (marked with a red rectangle in the

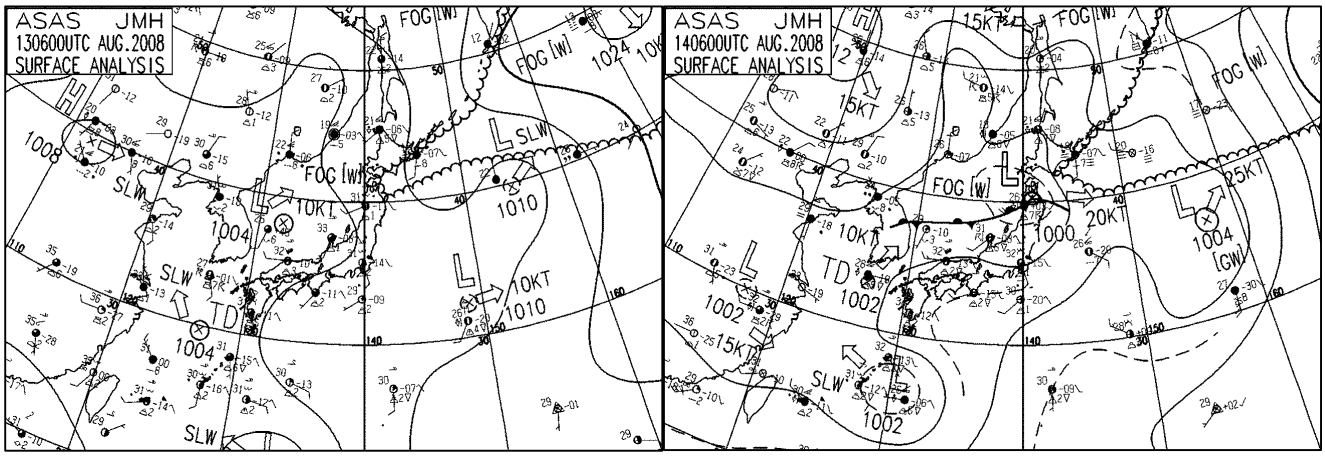

Fig. 17　The figure on the left is the weather chart for 0600 UTC on 13 August 2008 and the one on the right is for 0600 UTC on 14 August 2008

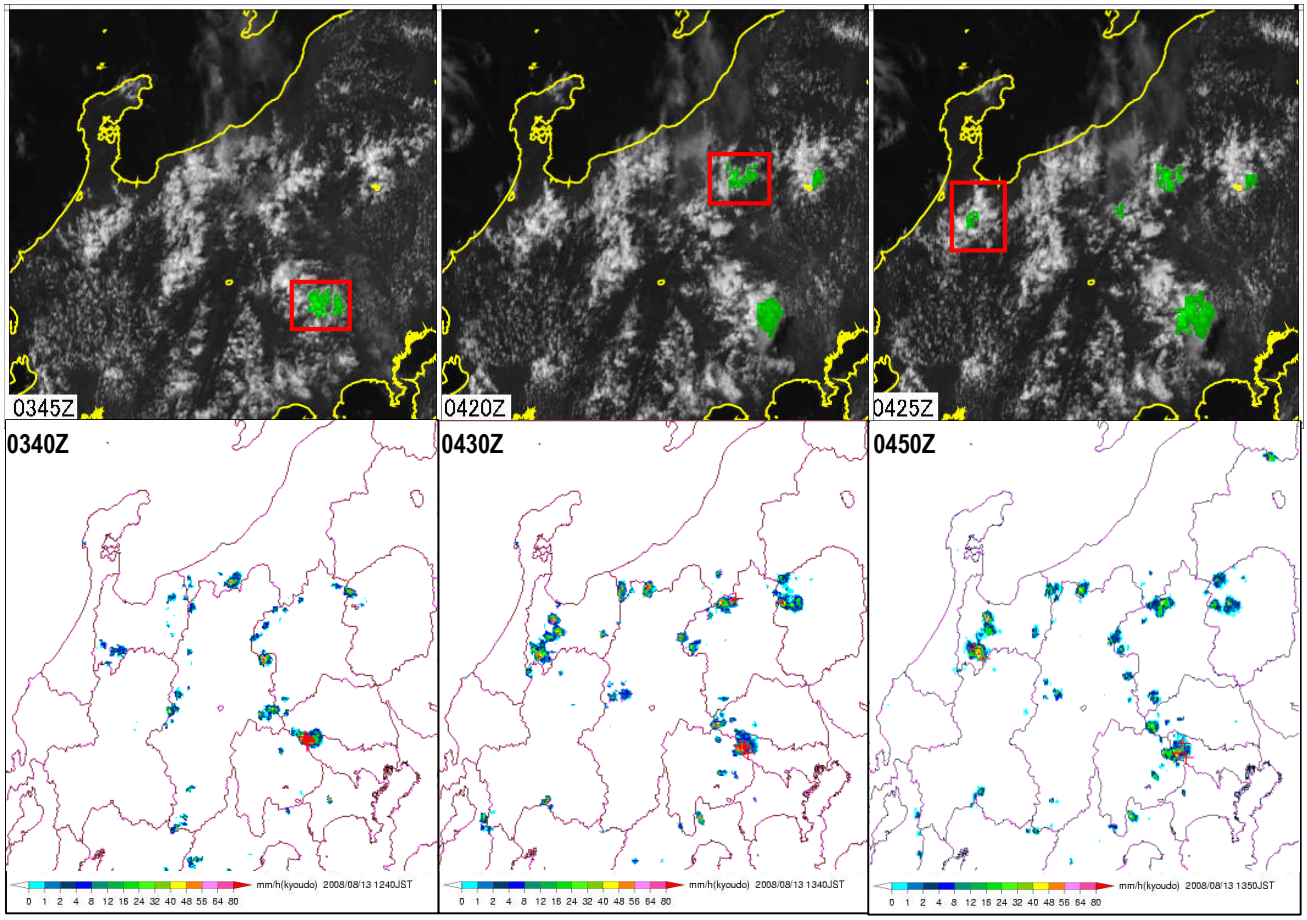

Fig. 18 The figures in the upper row are the same as the ones on the left in Fig. 10 but for the Kanto area at 0345, 0420, and 0425 UTC on 13 August 2008. The figures in the bottom row are the same as the ones on the right in Fig. 9(a) but for 0340, 0430, and 0450 UTC (the area depicted is the same as that shown in the figures in the upper row).

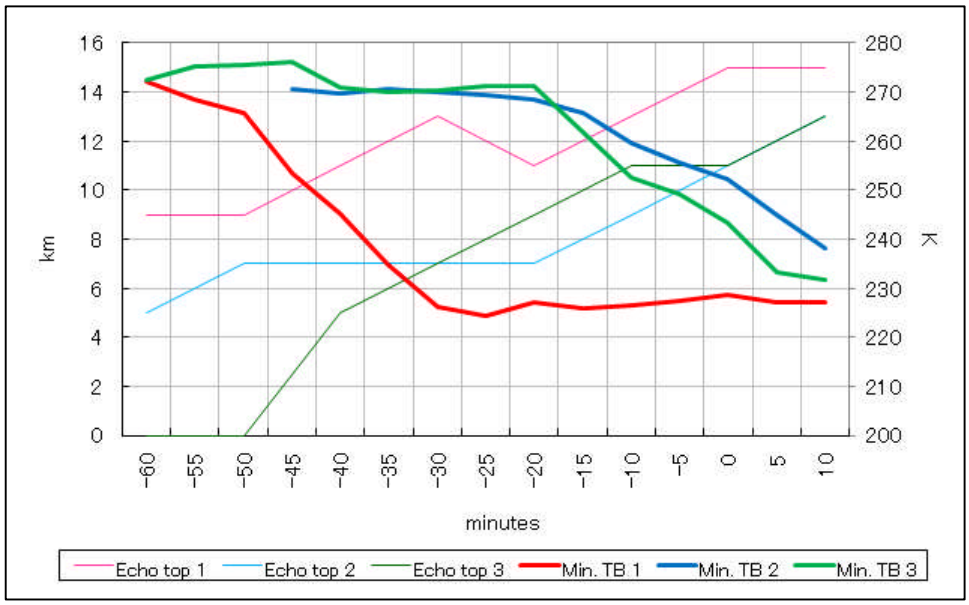

Fig. 19 Time series for echo top heights in km (thin curves) and the minimum TB IR 10.8 μm for the cloud-top in K (thick curves). The red and pink curves are for Cb_0330 on 16 July 2009, the blue curves are for Cb_0430 on 13 August 2008, and the green curves are for Cb_0520 on 14 August 2008.

upper left figure in Fig. 18), Cb_0430 in the northern part of Gunma prefecture (marked with a red rectangle in the upper middle figure in Fig. 18), and Cb_0450 in the southwestern part of Toyama prefecture (marked with a red rectangle in the upper right figure in Fig. 18). The SSI for Wajima at 0000 UTC was 0.3, and the SSI* was minus 2.1. The results for the 13 August 2008 case study are shown in the figures in the upper row of Fig. 18. Cb_0340 was not detected until 0345 UTC. The delay in its detection is because the condition 2-1 (the time trend for the TB of IR 10.8 μm) was not met. All of the other conditions were met from 0255 UTC. Cb_0430 was detected at 0420 UTC with a lead time of 10 minutes, while Cb_0450 was detected at 0425 UTC with a lead time of 25 minutes. These lead times were shorter than those for the case study described in section 5.1 were. The reason why Cb_0430 was not detected at 0415 UTC was also because condition 2-1 was not met. The time series for the minimum TB of IR 10.8 μm in the case of Cb_0430 and Cb_0330 on 16 July 2009 are shown in Fig. 19. The horizontal axis represents the time range based on the start of the thunderstorms. The minimum TB of IR 10.8 μm for the cloud-top of Cb_0430 begins to decrease about 20 minutes before it develops into a thunderstorm, and the echo top height begins to increase at the same time. However, the decrease rate is too small to meet condition 2-1. In addition to the lead time of the decrease of minimum TB of IR 10.8 μm, the average time trends for the minimum TB of IR 10.8 μm are very different for Cb_0430 and Cb_0330. The average time trend between minus 50 and minus 30 minutes for Cb_0330 is minus 2.0 K per minute. In contrast, the average time trend between minus 20 to 0 minutes for Cb_0430 is only minus 1.0 K per minute.

For this study, the data for 14 August 2008 was also researched. The weather chart for this date is shown in the figure on the right in Fig. 17. A stationary front extended from the Korean Peninsula to the northeast part of Japan. A cyclone near Okinawa Island was moving northwest, and a south-westerly wind was bringing warm and humid air to the low troposphere over the Kanto area. The values for the echo top heights and the minimum TB of IR 10.8 μm in the case of Cb_0520 on 14 August are depicted with green lines in Fig. 19. The average decrease rate for the minimum TB of IR 10.8 μm between minus 20 and 0 minutes was minus 1.4 K. The SSI, SSI*, and CAPE values for the three cases described in this section are shown in Table 5. The position of the maximum CAPE values are not fixed strictly with the target cells' spot; the maximum values around the cells were selected since the GPV data was believed to provide a good simulation of the weather condition pattern, but the geographical positions of convections are not fixed with that of the analysis data using observations (Fig. 20). The SSI and SSI* values were derived from radiosonde observations that were close to each cell. No correlation was identified between the decrease rate of minimum TB of IR 10.8 μm and either the SSI or the SSI* for any of the three cases. However, the decrease rate tended to be larger where the CAPE value was larger in these cases. It should be

Table 5　Instability values

Sample Name	Date	Observatory	Time	SSI	SSI*	Decrease Rate for MIN. TB IR 10.8	CAPE
Cb_0330	16 Jul. 2009	Kagoshima (31° 33′ 2N, 130° 32′ 8E)	00 UTC	-1.1	-2.8	-2.0	1000-1200
Cb_0430	13 Aug. 2008	Wajima (37° 23′ 5N, 136° 53′ 7E)	00 UTC	0.3	-2.1	-1.0	600-900
Cb_0520	14 Aug. 2008	Tateno (36° 03′ 4N, 140° 07′ 5E)	00 UTC	-2.9	-7.3	-1.4	900-1100

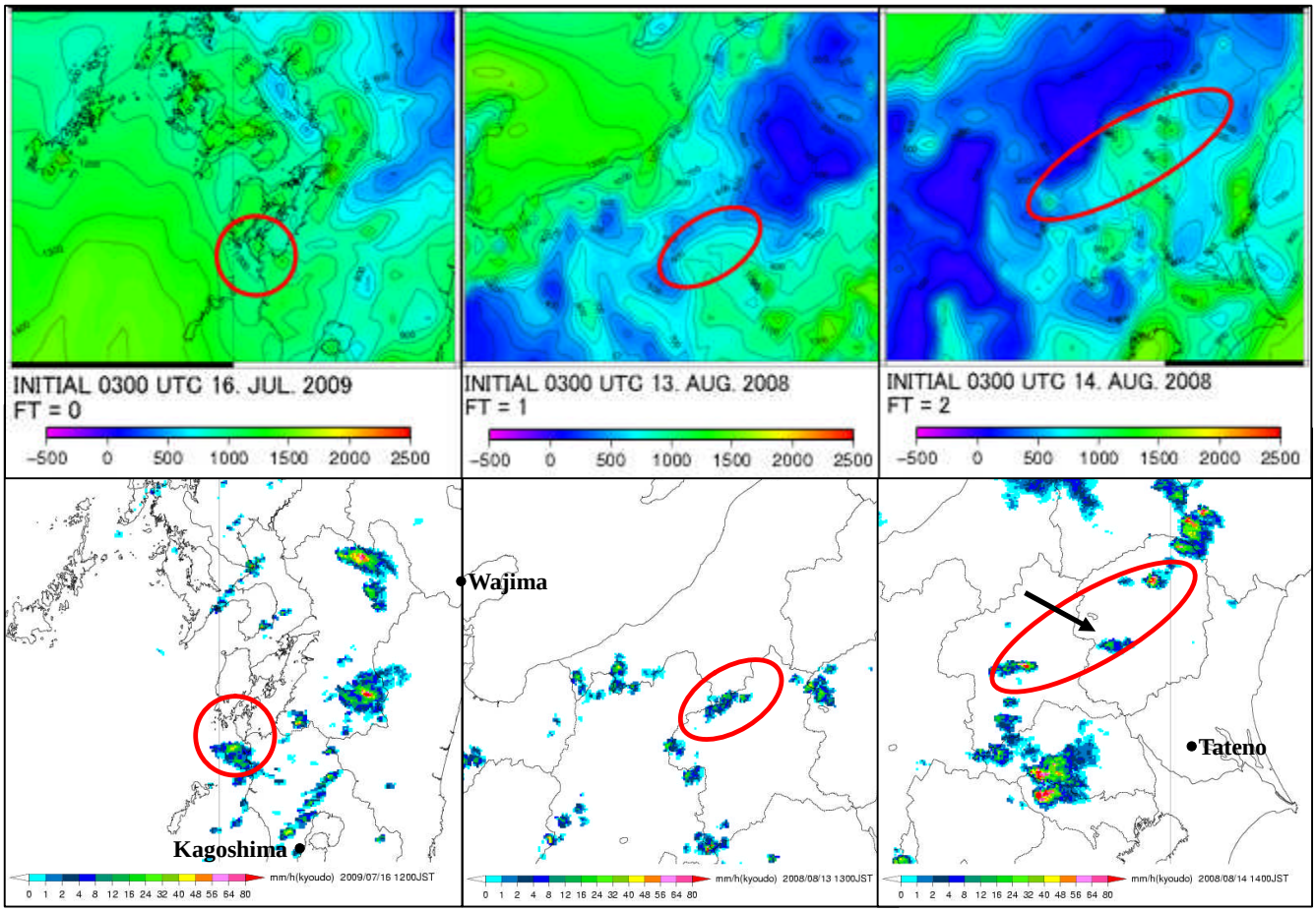

Fig. 20 The figures in the upper row show CAPE value distributions and those in the bottom show the precipitation intensity.

noted that, at present, this correlation has been verified for only three sample cases. This research will have to be continued using a much larger amount of RSO data in the future to confirm whether the best thresholds are dependent on the meteorological conditions.

6. Current state of research

This section describes the current state of research into the effectiveness of the Motion Cancellation process; provides an explanation of the slope index; and discusses the spatial lag between images from different channels that the satellite structure causes.

6.1 Effectiveness of the Motion Cancellation process

As was explained in section 3, the purpose of the Motion Cancellation process is to obtain accurate time trend parameters. Even when the Motion Cancellation process was not conducted, the results obtained using data for 16 July 2009 enabled the three cumulonimbus clouds discussed in section 5.1 (Cb_0300, Cb_0310, and Cb_0330) to be detected at the same time as was the case when the Motion Cancellation process was conducted (not shown). The probable reason for this is the definition of time trend parameters and the limited movement of the target clouds. If the movement of target clouds is too small relative to the template size, the Motion

Cancellation process proves ineffective. In this case, the average movement derived from the Motion Cancellation process was smaller than the template size.

Although omitting this process from the product will save time in terms of performing the calculations, such a decision should be made only after sufficient research has been conducted into the matter. The following is the course of action the developers plan to undertake in order to reach a decision on this. First, research will be conducted into cases when the target clouds were moving at higher speeds. The highest speed for the target clouds is assumed to be no more than 30 m/s, as explained below. If the Motion Cancellation process is found to be ineffective even for fast-moving clouds, it can be considered that omitting the process from this product will have no adverse effect. Second, the developers will reconsider the definitions for the time trend parameters. It is possible that the process is more effective if the maximum, minimum, or average values for the parameters are calculated for a smaller area.

6.2 Slope index

The slope index is an indicator of the updraft strength in convective clouds. As was explained in section 4, the index is available only when the TB of IR 10.8 μm of the

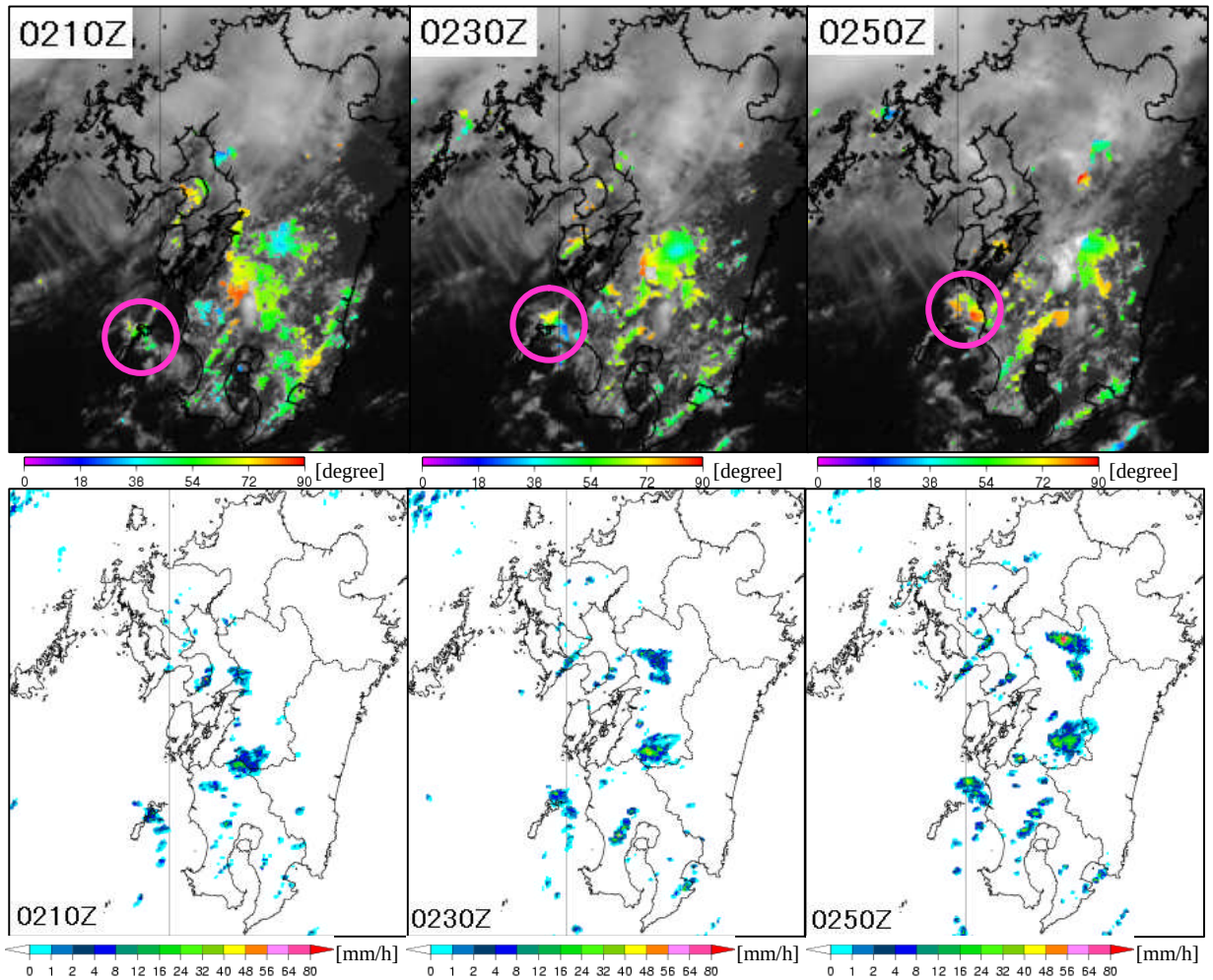

Fig. 21　The figures in the upper row show the slope index distributions for the Kyushu area at 0210 (left), 0230 (center), and 0250 (right) UTC on 16 July 2009. (The pink circles indicate the locations of Cb_0330.) The figures in the bottom row show the precipitation intensities for the same area and times as those depicted in the figures in the upper row.

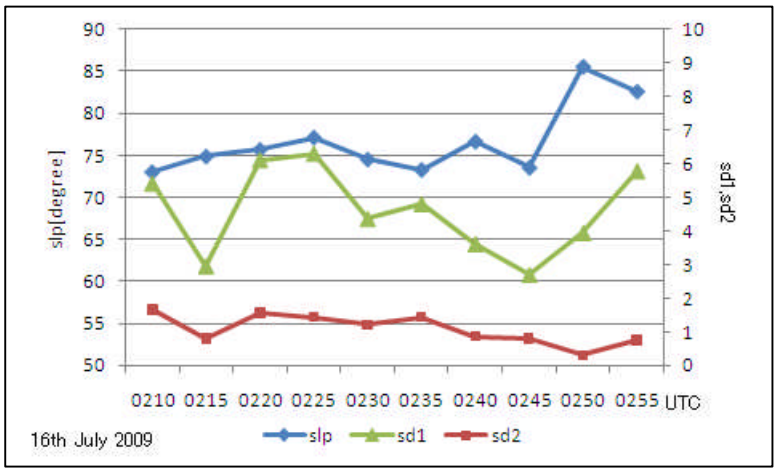

Fig. 22 Time series for the slope index (blue curve), the standard deviation of the TB as the numerator of the slope index (green curve), and the standard deviation of the effective radius as the denominator (red curve)

cloud tops is greater than 250 K. This section discusses how the slope index is an effective means of detecting RDCAs in the early stage of their lifecycles.

The target clouds for the 16 July 2009 case study had a high slope index. Figs. 21 and 22 show that the slope index for Cb_0330 was above 70 degrees from 0210 UTC. This value gradually increased while the TB of IR 10.8 μm was greater than 250 K. The denominator for this index is the standard deviation of the effective radius. Fig. 22 shows that the denominator tends to gradually decrease. In contrast, the numerator, which is the standard deviation of the TB of IR 10.8 μm, fluctuates between two and seven. In this case, the decrease in the standard deviation of the effective radius contributed to the increase in the slope index, and this decrease in the standard deviation of the effective radius reflects the logic introduced in section 4. Strong updrafts raise particles so fast that the radii of these particles do not differ greatly from those of particles in surrounding lower clouds. Given this, the features of the slope index in this case are summarized as follows.

1. The slope index is high for rapidly developing cumulus in the early stage of their lifecycles.
2. The slope index gradually increases while the clouds are developing.
3. The slope index's denominator gradually decreases.

These features were also found to hold true for Cb_0300 on 16 July 2009. The research of the slope index has started just recently. The other cases in various situations have to be investigated.

6.3 Spatial lag between images from different channels

There have been instances of spatial lag between satellite images from different channels. This is due to the structure of the satellite. The spatial lag for IR images obtained from MTSAT-2 are less than one pixel based on images at 10.8 μm. The lag for VIS images is less than 4 pixels. It is very difficult to estimate the spatial lag for images obtained from MTSAT-1R, since it depends on the geographic location and time. According to an estimation calculated using four hundred samples, the lag based on IR 10.8 μm is less than one pixel for other IR images and about four pixels for VIS images taken over Japan. Despite such spatial lags, when RDCA areas overlap for all channels, some grids in the overlap area will be detected. When more than one grid in a cumulus cloud meets all of the conditions, the entire cumulus area is regarded as an RDCA, as was explained in Section 3.4. Therefore, an acceptable lag is less than that of a cumulus cloud; namely, from several to 20 km or more. This is based on the order of the meso γ scale of 2 to 20 km. For the Motion Cancellation process and the time trend

parameters, the acceptable lag is less than a template size, which is larger than the estimated spatial lag.

7. Summary

This paper outlines a new product developed by the MSC/JMA for the detection of RDCAs using RSO data obtained from MTSAT-1R at five-minute intervals. RDCAs are cumulus cloud areas which are potentially expected to evolve into thunderstorms within one hour. The detection method employed for the RDCA product involves the following four processes: Detection 1; Motion Cancellation; Detection 2; and Consistency. In the Detection 1 process, candidate areas for RDCAs are detected by identifying developing cumulus cloud areas that have the potential to grow in height. The updraft strength is also checked. The Motion Cancellation process requires three successive images to calculate the time trend parameters used for the Detection 2 process. In the Detection 2 process, vigorously developing cumulus areas are detected from the candidate areas selected during the Detection 1 process. The time trend for the VIS albedo and that for the TB of IR 10.8 μm are used as parameters to estimate how vigorously the clouds are developing. The Consistency process has a purpose to ensure that critical Cbs remain marked while they are in the mature stages, as fully developed clouds are difficult to be detected in the preceding three processes. The Consistency process also helps to ensure that the detection results are consecutive, starting from the formation of a cloud area through to the occurrence of severe phenomena.

The results from the 16 July 2009 case study and the 12 to 14 August 2008 case study show that the RDCA product has a certain degree of suitability. The results for the 16 July 2009 case study showed that three target thunderstorms were successfully detected with a lead time of 20 to 50 minutes. The results, however, also showed some problems with the product. In section 5.2 (b), The SSI, SSI* and CAPE values for three Cbs were compared and discussed. It was found that the time trend for the TB of IR 10.8 μm tends to depend on the CAPE value; namely, that the larger the CAPE value was, the larger the time trend was in all three cases.

In Section 6, research into the effectiveness of the Motion Cancellation process was discussed and an explanation of the slope index was provided. The research included in this paper is insufficient to prove the effectiveness of the Motion Cancellation process. The slope index was found to have the potential to be an effective indicator for the detection of RDCAs in the early stages of cloud lifecycles.

The condition thresholds are currently decided subjectively based on an analysis of sample cases from 2008 and 2009. In addition, RSO data has been obtained from MTSAT-2. The MSC plans to re-evaluate these thresholds statistically using RSO data obtained from MTSAT-1R. As part of its mid-to-long range plan, the MSC are attempting to simulate satellite observations using Radiative Transfer Models. Using data that simulate various meteorological conditions, the developers expect to identify optimal thresholds and conditions for each meteorological pattern. This will provide various vertical profiles showing the situation throughout the whole of a cumulonimbus cloud’s lifecycle.

Acknowledgements

The authors would like to express their appreciation for the invaluable comments provided by Ms. Hiromi Owada, Mr. Kazuki Shimoji, Mr. Koutarou Saito, and Mr. Toshiharu Izumi of the JMA/MSC, Mr. Takanori Matsumoto and Naoki Tsukamoto of the JMA. They would also like to express their thanks for the insightful suggestions of the referee for this article.

References

Brotak, E., 2009: Nasty Surprise. J. A. Donoghue as editor-in-chief, AeroSafety World, October 2009, Flight Safety Foundation.

Lensky, I. M. and D. Rosenfeld, 2006: The time-space exchangeability of satellite retrieved relations between cloud top temperature and particle effective radius. Atmos. Chem. Phys., **6**, 2887-2894.

Lindsey, D. T., D. W. Hillger, L. Grasso, J. A. Knaff, and J. F. Dostalek, 2006: GOES Climatology and Analysis of Thunderstorms with Enhances 3.9-μm Reflectivity. Mon. Wea. Rev., **134**, 2342-2353.

Meteorological Satellite Center, Japan Meteorological Agency, 2002: The analysis and utilization of satellite images for aviation meteorology., 7-8, Meteorological Satellite Center (in Japanese).

Mouri, K., Y. Terasaka, 2008: Improvement of Satellite Cloud Grid Information using a Distinction Algorithm for Snow and Sea Ice Areas, Meteorological Satellite Center technical note, **51**, 57-72 (in Japanese)

Nakamura, Y., E. Ozawa, K. Onogi, and R. Kumabe, 2002: Impact experiments on NWP with Rapid Scan AMVs. Proc. **6**th International Winds Workshop, EUMETSAT, 171-178.

Oku, Y. and Ishikawa, H., 2008: Estimation of Reflectance and an Effective Radius of Cloud Particles Using MTSAT-1R Data. Annuals of Disas. Prev. Res. Inst., Kyoto Univ., No. **51B**, 409-415. (in Japanese)

Oyama, R., 2010: Upgrade of Atmospheric Motion Vector Derivation Algorithms at JMA/MSC. Meteorological Satellite Center Technical Note, **50**, 1-31.

Rosenfeld, D. and I. M. Lensky, 1998: Satellite-Based Insights into Precipitation Formation Processes in Continental and Maritime Convective Clouds. Bull. Amer. Meteo. Soc. **79**, 2457-2476.

Shimoji, K.,2010: The Development for MTSAT Rapid Scan High Resolution AMVs at JMA/MSC, Proceedings of the Tenth International Winds Workshop, Japan.

Sokal, R. R. and F. J. Rohlf, 1995: Biometry: The Principles and Practices of Statistics in Biological Research. 3rd edition, W. H. Freeman and Co., New York, 887, ISBN: 0-7167-2411-1.

Tokuno, M., 2002: Advanced Satellite Cloud Grid Information Data, Meteorological Satellite Center technical note, **40**, 1-24 (in Japanese)

MTSAT 高頻度衛星雲観測データを用いた
積雲急発達域の検出について

大坂　いづみ*、今井　崇人*、泉川　安志*

要　旨

気象衛星センターでは、急速に発達する積乱雲域を検出するためのプロダクトの開発を行っている。検出対象である積雲急発達域（Rapidly Developing Cumulus Area: RDCA）とは、急速に発達し一時間以内に発雷を伴う積乱雲になる雲領域である。プロダクト作成処理は、以下の 4 つの過程からなり、MTSAT-1R の高頻度衛星雲観測による 5 分間隔のデータが用いられる。検出第一過程、雲移動相殺過程、検出第二過程、一貫性保持過程である。検出第一過程は、積雲急発達域の候補としてまず発達期の積雲領域を抽出する目的がある。ここでは気象衛星センターの既存プロダクトである雲量格子点情報のアルゴリズムを一部参考にしている。雲移動相殺過程は、雲の移動を考慮した上で、雲の盛衰の指標となるパラメータの時間変化を算出するために組み込まれており、この時間変化量は次の第二検出過程で使用される。個の雲が持つパラメータの時間変化を算出するには、その雲の移動を特定した上で差分をとる必要がある。第二検出過程は、第一検出過程で絞られた候補領域から、雲移動相殺過程で算出されたパラメータの時間変化量を用いて急発達している領域のみを検出する過程である。この過程で用いられる時間変化量のうち、赤外 1 画像から作られるものは欧州気象衛星機構（EUMETSAT）の Convective Initiation（CI)プロダクトで使われているパラメータを参考に作成されている。可視画像から作られるものは本プロダクト独自のものである。一貫性保持過程は、最盛期を迎えた積乱雲域を検出する過程である。また、発達期に検出された雲が衰退し始めるまで安定して検出され続けるようにする役割もある。MTSAT-2 のデータを用いた数例の事例結果からは、このプロダクトの有効性が見られたが、同時に問題点もいくつか見受けられた。また本技術報告では、雲移動相殺過程及び slope index の有効性についての調査の途中報告、衛星チャンネル間の空間誤差に関する事項が報告されている。

*気象衛星センターデータ処理部システム管理課